

# Spin and Spin Entanglement in a Local-Realistic Model of Quantum Mechanics

Antonio Sciarretta

---

## Abstract

A realistic, stochastic, and local model for Quantum Mechanics (QM) has been presented in [1], aimed at reproducing non-relativistic QM results without using its mathematical formulation. Instead, the proposed model assumes only integer-valued quantities, in particular a discrete spacetime under the form of a lattice. The lattice plays the role of mediating the interactions between subsequent particles, giving rise to, e.g., interference phenomena. QM predictions are retrieved as probability distributions of similarly-prepared ensembles of particles. This paper focuses on the description of spin and spin entanglement, including the description of Stern-Gerlach apparatuses and Bell test experiments. Notably, it is shown that the proposed model, despite being local and realistic, is able to violate the Bell-CHSH inequalities by intrinsically renouncing to the measurement independence assumption.

---

## 1. Introduction

In [1, 2], we have proposed a model mimicking quantum mechanics (QM) with local, realistic, and stochastic features.

In the proposed model, the results of nonrelativistic spinless QM systems have been interpreted as probability distributions of similarly-prepared ensembles of particles that are emitted by one or multiple sources. At a given time, individual particles have definite values for position and momentum, among other observables, thus fulfilling *realism*.

The *stochastic* behavior that is manifested by the empirical evidence of QM is explained by assuming a fundamental randomness both in preparation and in particles trajectories. The emergence of QM behavior is a consequence of the particular rules of motion chosen. The motion of individual particles and their interaction with external forces take place on a discrete spacetime under the form of a lattice. Particle trajectories are asymmetric random walks, with transition probabilities being simple functions of a few quantities that are either randomly attributed to the particles during their preparation, or stored in the lattice nodes that the particle visits during the walk.

The lattice-stored information is progressively built as the nodes are visited by successive emissions. This process, where particles leave a “footprint” in the lattice that is used by subsequent particles, is ultimately responsible for the

QM behavior. Therefore the interactions between subsequent emissions fulfill *localism*, albeit through the mediation of the lattice. Interference and the Born rule emerge as a consequence of this mechanism.

In its nature, the proposed model could be regarded as the first full embodiment of the non-ergodic interpretation (NEI) proposed since the 1980s by V. Buonamano [3, 4]. The NEI idea was that, although separated by large time intervals, subsequent particles may interact with one another by means of memory effects in a medium (in our case, the lattice). That is, the usual assumption that time average coincide with ensemble averages is not true [5].

In this paper, we aim at extending the model to cover spin.

The main characteristics that distinguishes quantum spin from classical magnetic moment behavior is probably the quantization of the former after a measurement, e.g., by a Stern-Gerlach (SG) apparatus, is performed. This behavior is described in standard QM using matrices and eigenvectors. In alternative theories, spin has been derived from path integrals [6] and Nelson's stochastic mechanics [7, 8]. The local-realistic mechanism proposed here only involves a few additional quantities carried on by the particles. These variables are subject to stochastic preparation at sources and time evolution, including interaction with the lattice nodes storing the information about the magnetic field.

The proposed model is also used to demonstrate spin entanglement in addition to momentum entanglement already incorporated in [1]. Bell theorem is regularly used to dismiss any possibility that a local realist theory could explain spin entanglement results. This is because its main assumptions are the existence of hidden variables (“realism”) and locality. Rejecting either of the two leads to the standard approach of indeterminism (Copenhagen interpretation) or the non-standard approach of nonlocality (e.g., Bohm interpretation). However, Bell's theorem is also based on a third assumption, that of “measurement independence” (MI) that is rather strong. The fact that MI is not satisfied have been often explained by some kind of (super)determinism or “conspiracy”. However, other, less unpleasant reasons to renounce to MI exist.

Although non-ergodic solutions would in principle belong to this category, no proposal has been issued in this direction as per the best knowledge of the author [9]. In [10] a toy contextual model for which MI is not satisfied is presented. Other attempts include the use of negative probabilities [11], or heuristic models that correctly reproduce the QM correlations by renouncing to MI in an abstract and physically unexplained fashion [12]. A different approach is to renounce to the “fair detection” assumption and assume instead that the probability of joint detection (detector efficiency) depends on the settings [13, 4].

However, the most interesting attempt to reproduce Malus' law and QM predictions in a local-realistic context seems the event-based class of models proposed by [14, 15]. In this approach, the key role is played by the time delay between particle arrivals at the detectors of a Bell-type experiment, so that coincidences are counted only if two particles arrive at roughly the same time. Such a time delay is heuristically designed and explained with the properties of the apparatus. In the proposed model, the time-of-fly plays a similar role in determining coincidences to be counted. However, it is a natural consequence of

the rules of motion in the presence of magnetic forces and a stochastic quantity due to stochastic preparations.

The paper is organized as follows. In Sect. 2 a summary of the three-dimensional spinless model is presented, with some additional considerations with respect to [1]. Then in Sect. 3 the additional rules for spin 1/2 are introduced, both for homogeneous and inhomogeneous (SG) fields. These results are extended to higher spins in Sect. 4. Two-particle spin entanglement is discussed in Sect. 5.

## 2. Summary of the Local-Realistic Model for a Spinless Particle

In this section, we summarize the rules for particle emissions (Sect. 2.1), microscopic motion (Sect. 2.2), and how probability densities are derived from them (Sect. 2.3). The reader is referred to [1] or its companion paper [2] for more detail.

### 2.1. Lattice and particle emissions

The lattice is composed of three spatial dimensions  $x = \{x_d\} \in \mathbb{Z}^3$ , and one temporal dimension  $n \in \mathbb{N}$ . Each of the spatial dimensions is characterized by the same fundamental length and acts independently.

We describe ensembles of particles that are emitted at some sources after having been similarly prepared. Source setting consists in defining the number of sources  $N_s$ , their location  $x_0^{(k)}$ , probabilities  $P_0^{(k)}$  (such that  $\sum_k P_0^{(k)} = 1$ ), and phase  $\epsilon^{(k)}$ , with  $k \in [1, N_s]$ .

Each particle is emitted from one source, randomly chosen among those available according to their probabilities. Thus source preparation fixes the source position  $x_0 = \{x_{0d}\} \in \mathbb{Z}^3$  and the source phase  $\epsilon = \{\epsilon_d\} \in \mathbb{Q}^3$ . Additionally, the source momentum  $v_0 = \{v_{0d}\} \in \mathbb{Q}^3$ , and the source (momentum) polarization  $\rho = \{\rho_d\} \in \mathbb{Q}^3$  are randomly attributed to the particle. The latter two quantities are further subject to the conditions  $\sum_{d=1}^3 \rho_d^2 = 1$ ,  $\sum_{d=1}^3 v_{0d}^2 \leq 1$ .

### 2.2. Microscopic motion

Microscopic motion is defined by a set of rules involving quantities carried by particles and quantities carried by lattice node (subscript  $xt$ ).

The particle-carried quantities (or “counters”) are: its span  $\ell = \{\ell_d\} \in \mathbb{Z}^2$ , lifetime  $t \in \mathbb{N}$ , momentum  $v = \{v_d\} \in \{-1, 0, 1\}^3$ , momentum propensity  $\mathbf{v} := \mathbb{E}[v]$ , “energy”  $e := \mathbb{E}[v^2]$ , quantum momentum  $v_Q = \{v_{Qd}\} \in \mathbb{Q}^3$ , momentum due to external forces  $v_F = \{v_{Fd}\} \in \mathbb{Q}^3$ .

Particles exchange momentum-mediating entities called “bosons” with the lattice, according to the mechanism illustrated below. External-force bosons (FB) carry a momentum  $f = \{f_d\} \in \mathbb{Q}^3$ , while quantum particle bosons (PB) carry momenta  $w^{(\cdot)} \in \mathbb{Q}$  and their own lifetime  $t^{(\cdot)}$ .

The particle's motion rules are summarized as

$$t[n] = t[n-1] + 1, \quad t[n_0] = 0 \quad (1)$$

$$\ell_d[n] = \ell_d[n-1] + v_d[n], \quad \ell_d[n_0] = 0 \quad (2)$$

$$x_d[n] = x_{0d} + \ell[n] \quad (3)$$

$$\mathbb{P}(v_d[n] = \pm 1) = \frac{e_d[n] \pm \mathbf{v}_d[n]}{2}, \quad \mathbb{P}(v_d[n] = 0) = 1 - e_d[n] \quad (4)$$

$$e_d[n] = \frac{1 + \mathbf{v}_d^2[n]}{2} \quad (5)$$

$$\mathbf{v}_d[n] = v_{Qd}[n] + v_{Fd}[n] \quad (6)$$

$$v_{Fd}[n] = \sum_{n'=n_0+1}^n f_d(x[n'], n') \quad (7)$$

$$v_{Qd}[n] = v_{0d} - \rho_d^2 \sum_{\ell} \sum_{\lambda \neq \ell} w^{(\ell\lambda)}[n] \quad (8)$$

$$w^{(\ell\lambda)}[n] = w^{(\ell\lambda)}[n-1] \cdot \left(1 - \frac{1}{2t^{(\ell\lambda)}}\right) \quad (9)$$

where  $n_0$  is the iteration at which the emission has taken place.

Equations (1)–(3) describe the increments of lifetime, span, and position as a function of momentum. Equations (4)–(5) relate the probability distribution of momentum to momentum propensity. Equation (6) states that momentum propensity is the sum of two contributions, due to quantum and external forces, respectively. External forces are described by interactions with the lattice, where each node can be occupied by a force boson. When a particle visits the node, it captures the resident FB and incorporates its momentum as described in (7). A new boson is then recreated at the node. In (19), quantum momentum is initially set to the source momentum and then build up from an exchange of bosons and their momenta between the particle and the lattice. The dynamics of the PB-momentum is given in (9).

Lattice-carried quantities are the span trace  $\lambda_{xt} = \{\lambda_{d,xt}\} \in \mathbb{Z}^3$  and the phase trace,  $\epsilon_{xt} \in \mathbb{Q}^3$ , which represent the memory of the span and phase carried by the last particle that has visited the node  $x$  with lifetime  $t$ . Additionally, the exchange with particles generate quantum lattice bosons (LB), carrying momenta  $\omega_{xt}^{(\cdot)} \in \mathbb{Q}$ , whose dynamics read

$$\omega_{xt}^{(\ell\lambda)}[n] = \omega_{xt}^{(\ell\lambda)}[n-1] \cdot \left(1 - \left(\frac{\omega_{xt}^{(\ell\lambda)}[n_{QR}]}{t^{(\ell\lambda)}}\right)^2\right). \quad (10)$$

Rules (1)–(10) are partially overcome in case of a quantum reset or an external reset. A Quantum Reset (QR) occurs when  $\ell_d \neq \lambda_{d,xt}$  for at least one

dimension  $d$ . If it is the case, the following exchanges apply:

$$w^{(\ell\lambda)} \xleftarrow{QR} \frac{\omega_{xt}^{(\ell\lambda)}}{\sum_{d=1}^3 \rho_d^2 \delta_d^{(\ell\lambda)}} \quad (11)$$

$$\omega_{xt}^{(\ell\lambda)} \xleftarrow{QR} \sum_{d=1}^3 \delta_d^{(\ell\lambda)} v_{Qd} - \epsilon^{(\ell\lambda)} \quad (12)$$

$$\ell_d \xleftrightarrow{QR} \lambda_{d,xt} \quad (13)$$

$$\epsilon \xleftrightarrow{QR} \epsilon_{xt} \quad (14)$$

where  $\delta_d^{(\ell\lambda)} := |\ell_d - \lambda_{d,xt}|$  is the path difference and  $\epsilon^{(\ell\lambda)} := \epsilon - \epsilon_{xt}$  is the phase difference.

Rules (11)–(12) state that the QR creates a new momentum-carrying LB, labeled  $\ell\lambda$  to unambiguously identify the information carried by the particle, resp., the lattice node. The new LB replaces the old one of the same type, which is transferred to the particle and becomes a particle boson (PB). Rules (13)–(14) describe the exchange of counters between the particle and the lattice.

An External Reset (ER) occurs when an external-force boson is captured, and is defined by the rules

$$v_{d0} \xleftarrow{ER} v_d \quad (15)$$

$$\ell_d \xleftarrow{ER} \ell_d - 2f_d \frac{\sum_{d'=1}^3 \ell_{d'} f_{d'}}{\sum_{d'=1}^3 f_{d'}^2} \quad (16)$$

$$\epsilon \xleftarrow{ER} \epsilon + 1. \quad (17)$$

Although not necessary, rule (15) is introduced here for the sake of model elegance. It states that each ER can be seen as a new emission, thus removing the special role of sources that are now seen as just the nodes where the last interaction has taken place. Rule (16) generalizes the 1D situation where the span's sign is inverted at each external interaction. Rule (17) adds a  $\pi$  phase angle after each interaction.

### 2.3. Probability densities

The source position, momentum, and polarization are treated as random variables. In particular, the probability density function of the source momentum is  $\rho(v_{0d}) = (1/2)$ ,  $\forall d$ .

Stochastic preparation implies that  $\mathbf{v}$  and thus  $x$  are random variables, too. We aim at evaluating the probability mass function of the position for an ensemble of similarly-prepared particles. Unfortunately, it is generally not possible to explicitly evaluate  $\rho(x;t)$ . However, as discussed in [1], for sufficiently large times we can use the approximation  $\rho(x;t) \approx \rho(\mathbf{x};t)$ , where  $\mathbf{x} \in \mathbb{R}$  is the expected value of the position<sup>1</sup>.

---

<sup>1</sup>We shall generally denote expected values with bold letters.

We describe in the rest of this section the procedure to evaluate the joint pdf's  $\rho(\mathbf{x}; t)$  and  $\rho(\mathbf{v}_Q)$  in the presence of quadratic potentials, potential barriers, or geometrical constraints.

### 2.3.1. Quadratic potentials

It was shown in [1] that, in case of a quadratic potential, the expected motion is given by

$$\mathbf{x}_d = A_d(t)x_{0d} + B_d(t)\mathbf{v}_{Qd} + C_d(t) \quad (18)$$

and

$$\mathbf{v}_{Qd} = v_{0d} - \rho_d \sum_i \sum_{j \neq i} \sqrt{P_0^{(i)} P_0^{(j)}} \frac{\sin(arg)}{\pi \sum_{d=1}^3 \rho_d \delta_d^{(ij)}} \quad (19)$$

$$(arg) = \pi \sum_{d=1}^3 \delta_d^{(ij)} \frac{\mathbf{x}_d - A_d(t) \frac{x_{0d}^{(i)} + x_{0d}^{(j)}}{2} - C_d(t)}{B_d(t)} - \pi \epsilon^{(ij)}. \quad (20)$$

where  $A(t)$ ,  $B(t)$ , and  $C(t)$  are functions of lifetime whose form depends on the FB momentum (external force)  $f(x, t)$ . For example, a free particle is described by  $A = 1$ ,  $B = t$ ,  $C = 0$ ; a free faller by  $A = 1$ ,  $B = t$ ,  $C = ft^2/2$ ; an harmonic oscillator by  $A = \cos \Omega t$ ,  $B = \sin \Omega t / \Omega$ ,  $C = 0$ .

The joint pdf of the positions is found by applying the rule

$$\rho(\mathbf{x}; t) = \frac{1}{2} \left| \frac{\partial(v_{01}, \dots, v_{03})}{\partial(\mathbf{x}_1, \dots, \mathbf{x}_3)} \right|, \quad (21)$$

yielding

$$\rho(\mathbf{x}; t) = \frac{1 + \sum_i \sum_{j \neq i} \sqrt{P_0^{(i)} P_0^{(j)}} \cos(arg)}{\prod_{d=1}^3 2|B_d(t)|} \quad (22)$$

In [1] it was shown as well that the Schrödinger equation and Born rule can be retrieved from (22).

Similarly, the joint pdf of the momenta is evaluated as

$$\rho(\mathbf{v}_Q; t) = \frac{1}{2^3} \left( 1 + \sum_i \sum_{j \neq i} \sqrt{P_0^{(i)} P_0^{(j)}} \cos \left( \pi \sum_{d=1}^3 \delta_d^{(ij)} \mathbf{v}_{Qd} - \pi \epsilon^{(ij)} \right) \right). \quad (23)$$

Note that the expected-motion equations (18)–(20) can be used, alongside with the source settings, as an approximated version of the model to accelerate numerical simulations<sup>2</sup>.

---

<sup>2</sup>As explained in [2], the quantum momentum should be filtered by a first-order lag before inserted in (19) in order to avoid numerical instabilities and represent the non-instantaneousness of the training process.

### 3. Spin $\frac{1}{2}$

A spin mechanism is now superimposed to the microscopic motion mechanism treated in the previous sections. The momentum quantities  $v_0$  and  $v$  have their spin counterparts  $s_0$  and  $s$ . The (momentum) polarization  $\rho$  has its spin counterpart in the (spin) polarization  $\mu$ . The latter two quantities might actually coincide: at the present stage of the model development, we do not have reasons to distinguish them but for their naming.

#### 3.1. Microscopic motion

Particles are emitted with additional, randomly-attributed properties denoted as “source spin”,  $s_0 \in [-1, 1]$  and “source polarization”,  $\mu_0 := \{\mu_{0d}\} \in \mathbb{Q}^3$ , such that  $\sum_{d=1}^3 \mu_{0d}^2 = 1$ .

While  $s_0$  remains constant during a particle’s evolution, polarization is prone to change at each time the particle experiences a magnetic field, which is represented under the form  $B := \{\lambda_d\}B_M$ , such that  $\sum_{d=1}^3 \lambda_d^2 = 1$ . Clearly,  $\lambda$  represents the unit vector along which the physical field is directed. The quantity  $B_M$  represents the magnitude of the magnetic field in lattice units.

The evolution of the polarization follows the rule

$$\mu_d[n + 1] = \mu_d[n] - \gamma\mu_M B_M (\mu_{d+1}[n]\lambda_{d+2}[n] - \mu_{d+2}[n]\lambda_{d+1}[n]) \quad (24)$$

with  $\mu_d[n_0] = \mu_{0d}$ . The quantity  $\mu_M$  represents the magnitude of the magnetic moment of the particle, and the dimension indexes must be taken as modulo three. The quantity  $\gamma$  represents the gyromagnetic ratio. Note that, if the  $\lambda_d$ ’s are constant, the sum  $\sum_d \mu_d^2$  is constant, too. Similarly, the sum  $M := \sum_d \mu_d \lambda_d$  does not change with iterations if the field is constant<sup>3</sup>. We also define for later use  $M_0 := \sum_d \mu_{0d} \lambda_d$ .

The quantity denoted here as spin is a bivalued quantity  $s \in \{-1, 1\}$  that varies during the particles evolution according to the rule

$$s[n] = \text{sign}(s_0 + M[n]) . \quad (25)$$

Clearly, the expected value of spin  $\mathbb{E}[s[n]] = M[n]$ . For such reason, we shall denote the quantity  $M$  as “spin propensity” in the following.

Assuming that  $\lambda$  is constant, the magnetic force (external boson momentum) due to spin is described in analogy to the classical expression,

$$f_d[n] = -\mu_M \sum_{d'=1}^3 \mu_{d'}[n] \frac{\partial B_M}{\partial x_d}[n] \lambda_{d'}[n] . \quad (26)$$

We shall assume for later use that  $B_M$  is parameterizable as  $\partial B_M / \partial x_d := B_F \nu_d$ , with  $\sum_{d=1}^3 \nu_d^2 = 1$ . The force is thus directed along the  $\nu := \{\nu_d\}$  direction and we can define its magnitude as  $f_\nu[n] = -\mu_M B_F M[n]$ .

---

<sup>3</sup>The quantity  $M$  clearly corresponds to the cosine of the angle between the two directions  $\mu_0$  and  $\lambda$ .

When an external boson is captured, besides the actualization of its momenta and spans (15)–(17), the particle undergoes an External Reset (ER) of its polarization,

$$\mu_d \xleftarrow[\text{ER}]{} s\lambda_d . \quad (27)$$

This reset causes an instantaneous variation of the spin propensity, that jumps to the current spin. In analogy with classical physics, we define a “magnetic energy”  $\mathcal{E} := -\mu_M B_M M$ . The variation of magnetic energy across the ER is compensated by a reset of momentum propensity in the direction perpendicular to force, which is described by the rules

$$\mathbf{v}_d \xleftarrow[\text{ER}]{} \alpha \mathbf{v}_d + (1 - \alpha) \nu_d \sum_{d=1}^3 \mathbf{v}_d \nu_d , \quad (28)$$

$$\alpha^2 = \frac{\sum_d \mathbf{v}_d^2 - \mu_M B_M (s - M)}{\sum_d \mathbf{v}_d^2} . \quad (29)$$

### 3.2. Probability densities

We aim at evaluating the pmf  $\rho(s)$ , which results from the particular preparation at the source and the nature of the magnetic field experienced by the ensemble of particles. We shall consider first a preparation (“pure state”) for which the source polarization has a definite value  $\mu_0$  for all the particles of the ensemble.

#### 3.2.1. Homogeneous field

If the magnetic field  $B_d = B_M \lambda_d$  is homogeneous in space (though possibly variable with time), no magnetic force is experienced, thus no external reset occurs. If the field is also constant,  $M$  does not change with the iterations and thus is always equal to its initial value,  $M[n] \equiv M_0$ .

From (25), we have that  $s$  is also constant as

$$s[n] = \begin{cases} 1, & s_0 > -M_0 \\ -1, & s_0 < -M_0 \end{cases} . \quad (30)$$

Since  $s_0 = U[-1, 1]$ , the probabilities of spins up and down are evaluated as

$$\rho(\pm 1) = \mathbb{P}(s = \pm 1) = \frac{1 \pm M_0}{2} = \frac{1 \pm \cos(\mu_0, \lambda)}{2} , \quad (31)$$

and is easily generalized to the case of a variable field, in perfect agreement with QM prediction.

The meaning of the polarizations in the model can be now clarified. If the field is along one particular direction  $d$ , then  $\lambda_d = 1$ , and consequently  $\rho(1) = (1 + \mu_d)/2$ ,  $\rho(-1) = (1 - \mu_d)/2$ . The expectation of the spin is therefore  $\mathbf{s} = (1)(1 + \mu_d)/2 + (-1)(1 - \mu_d)/2 = \mu_d$ . Thus the  $d$ -polarization represents the standard QM quantity  $\langle S_d \rangle$ , that is, the expected value of the spin measured along the  $d$  direction.



It should be also apparent that the standard QM spinor formulation of a spin state can be retrieved by defining the complex vector quantity

$$\chi = \left( \sqrt{\frac{1 + \mu_3}{2}}, \frac{\mu_1 - i\mu_2}{\sqrt{2}\sqrt{(1 + \mu_3)}} \right)^T. \quad (32)$$

from which all standard results can be obtained.

### 3.2.2. 1D-inhomogeneous field (Stern-Gerlach apparatus)

We shall consider now the case where the prepared particles pass through a Stern-Gerlach apparatus. Inside this apparatus, the field has a prevalent magnitude  $B_M$  along a constant direction  $\lambda$  and some small inhomogeneity inducing a magnetic force of magnitude  $\mu_M B_F$  along the constant direction  $\nu$ .

Outside the SG,  $\lambda = 0$ ,  $\mu \equiv \mu_0$ , and so is  $M = 0$ . Thus, spins up and down are equally distributed. Let us define  $n_i$  as the iteration at which particles enter the SG. The spin propensity becomes  $M[n_i] = M_0$ . Thus, the probability distribution of  $s[n_i]$  follows (31).

The presence of a magnetic force in the SG activates the External Reset condition. We shall assume, for the sake of discussion only, that each node inside the SG hosts a magnetic-force boson and thus the first ER occurs right at the SG entry at  $n_i$ . Then,

$$M \stackrel{\text{ER}}{\leftarrow} s \sum_{d=1}^3 |\lambda_d|^2 = s, \quad (33)$$

that is, the spin propensity “jumps” to the current spin value. At the immediately next iteration, the application of (25) states that  $\mathbb{P}(s[n_i + 1] = \sigma) = (1 + \sigma s[n_i])/2$ . In other words, if  $s[n_i] = 1$ , then  $s[n_i + 1]$  will be 1 with probability one. Inversely, if  $s[n_i] = -1$ , then  $s[n_i + 1]$  will surely remain -1. At successive ER’s, the situation does not change and thus the spin remains constant throughout the whole SG apparatus. The probability of having spins up or down, respectively, at the SG exit is thus still given by (31),

$$\rho(s) = \frac{1 + s \cos(\mu_0, \lambda)}{2}. \quad (34)$$

### 3.2.3. Cascade of SG’s

In textbook descriptions of spin, two or more SG apparatuses in series are often employed to illustrate its non-classical properties.

In the proposed model, particles having spin  $s_1 = \pm 1$  at the output of the first SG have also polarization  $\mu = \pm \lambda_1$ . At the entry of the second SG, the spin propensity is thus  $M = s_1 \sum_d \lambda_{1d} \lambda_{2d}$ . Using the result of the previous section, the probability of spins up or down at the exit of the second SG is evaluated as

$$\rho(s_2|s_1) = \frac{1 + s_2 s_1 \cos(\lambda_1, \lambda_2)}{2}, \quad (35)$$

again in perfect agreement with standard QM calculation.

### 3.3. SG simulation and numerical results

We shall consider a magnetic field concentrated in a certain region of space along the propagation direction  $x_2$  and oriented along the  $x_3$  axis, with a one-dimensional inhomogeneity along the same direction,  $B = (0, 0, B_1 x_3)$ . Even if this field does not satisfy Maxwell equation  $\nabla \cdot B = 0$ , we choose it to simplify the notation. In fact, the literature has shown its equivalence to any “physical” field where the inhomogeneity is along one constant direction, provided that the two directions are exchanged [16].

In the proposed model, particles are emitted at the source according to a Gaussian-wave preparation. To represent a Gaussian wave with zero mean and variance  $(N_s - 1)/4$ ,  $N_s$  sources are set at adjacent nodes centered at  $x = 0$ . The source probability and phase are set as

$$P_0(x) = \frac{1}{2^{N_s-1}} \binom{N_s-1}{x + \frac{N_s-1}{2}}, \quad \epsilon_d(x) = mx, \quad (36)$$

with  $m \in [0, 1]$  and  $(\cdot)$  representing here a binomial coefficient.

To represent the SG scenario, we have set  $m_1 = m_3 = 0$ , while  $m_2$  would determine the average particle speed along the propagation direction. We assume that the time spent before encountering the SG is sufficient to complete both the “lattice training” and the “particle training” processes discussed in [1], and we simulate the expected-motion version of the model, equations (18)–(20), as explained in Sect. 2.3. When (23) is applied to (36), one obtains a momentum pdf that approximates a Dirac delta centered around the phase momentum,  $\rho(v_Q) \approx \delta(v_Q - m)$ . From (18), it follows that  $\mathbf{x}_d \approx m_d t$ . We shall take this approximation as exact for the direction of propagation, and posit  $x_3 = m_3 t$ , thus limiting our analysis to the plane perpendicular to propagation.

By virtue of the equivalence (32), the initial polarizations are chosen as to represent an initial spin state  $\chi_0 = (\chi_1, \chi_2)$ ,

$$\mu_{03} = \chi_1 \chi_1^* - \chi_2 \chi_2^*, \quad \mu_{01} = \chi_1 \chi_2^* + \chi_1^* \chi_2, \quad \mu_{02} = -i(\chi_1 \chi_2^* - \chi_1^* \chi_2), \quad (37)$$

where the asterisk denotes here complex conjugation.

Ensemble results are compared with those of quantum mechanics (theoretical values) obtained by using the two-component propagator [16, 17]

$$K^{(SG)}(x, t|x_0) = \frac{1}{(2it)^{3/2}} \cdot \exp\left(\frac{i\pi(x-x_0)^2}{2t} + \frac{i\pi(x_1+x_{01})\sigma_3\phi t}{2} - \frac{i\pi\phi^2 t^3}{24}\right) \quad (38)$$

in lattice units, where  $\sigma_3$  denotes here the third Pauli matrix.

The theoretically expected pdf is obtained numerically from the propagated spinor  $\chi(x, t)$  as  $\rho(x; t) = \chi^\dagger \begin{pmatrix} 1 & 0 \\ 0 & 1 \end{pmatrix} \chi$ . This pdf is to be compared with the frequency of particle arrivals at nodes  $x$  after  $t$  iterations computed by the average-motion model. The theoretically expected spin density is obtained as  $\langle S_3 \rangle(x; t) = \chi^\dagger \begin{pmatrix} 1 & 0 \\ 0 & -1 \end{pmatrix} \chi$ . This quantity is to be compared with its counterpart in the proposed model, obtained as the difference between the frequency

of arrivals of particles with  $s = 1$  ( $\mu_3 = \lambda_3 = 1$ ) and of those with  $s = -1$  ( $\mu_3 = -\lambda_3 = -1$ ).

Figures (1)–(2) show the calculated spin density after  $t = 64$  iterations for a source scenario with  $\mu_M B_F = 0.1/\pi^2$ ,  $d_1 = d_2 = 1$ ,  $\chi_1 = \chi_2 = 1/\sqrt{2}$  (that is,  $\mu_{01} = 1$  in the proposed model). Globally, these result match the theoretical values, which clearly show the “textbook” spin separation occurring along the inhomogeneity direction.

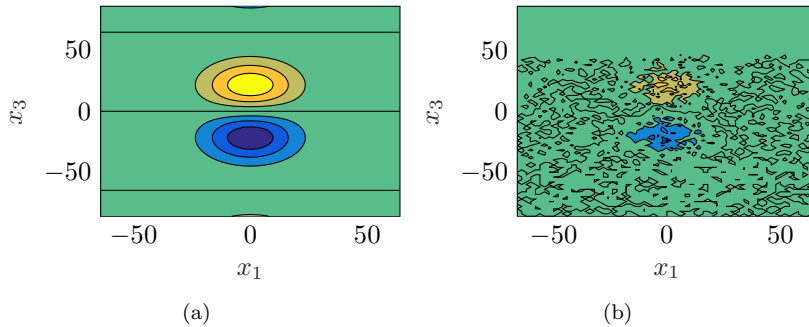


Figure 1: Differential frequency of arrival (b) and theoretical spin density  $\langle S_3 \rangle$  (a) for  $N_p = 10000$ ,  $t = 64$  as a function of position (Stern-Gerlach, Gaussian wave,  $\mu_M B_F = 0.1/\pi^2$ ,  $d_1 = d_3 = 1$ ,  $\chi_1 = \chi_2 = 1/\sqrt{2}$ ).

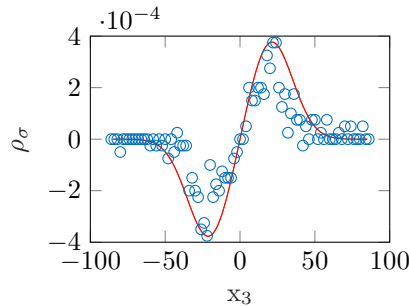


Figure 2: Differential frequency of arrival (blue) and theoretical spin density (red) for  $N_p = 10000$ ,  $t = 64$  as a function of the inhomogeneity direction (Stern-Gerlach, Gaussian wave,  $\mu_M B_F = 0.1/\pi^2$ ,  $d_1 = d_3 = 1$ ,  $\chi_1 = \chi_2 = 1/\sqrt{2}$ ).

#### 4. Higher spins

In this section we extend the model to particle having spin  $S$  higher than  $\frac{1}{2}$ . For particles with general spin number  $S$  ( $S = 1/2, 1, 3/2, \dots$ ), the quantity here denoted as spin ( $s$ ) can take  $2S + 1$  values equispaced between  $+1$  and  $-1$  ( $s \in [1, 1 - 1/S, \dots, -1]$ ).

#### 4.1. Microscopic motion

In addition to their source spin and  $\mu$ -polarization, particles are emitted with a second polarization vector (third, including  $\rho$ )  $\tau_0 := \{\tau_{0d}\} \in \mathbb{Q}^3$ . The constraint on polarization components is generalized as

$$\sum_d \mu_{d0}^2 = \tilde{s}_0^2, \quad \sum_d \tau_{d0}^2 = \frac{S+1}{S} - \tilde{s}_0^2, \quad (39)$$

where  $\tilde{s}_0$  denotes the spin-rounded value of  $s_0$ ,  $\text{Round}(S(1+s_0))/S-1$ . Clearly, for  $S = 1/2$ , one retrieves  $\tilde{s}_0 = \pm 1$  and  $\sum_d \mu_{d0}^2 = 1$ .

To describe the dynamics of polarization, equation (24) still holds when applied to both vectors  $\mu$  and  $\tau$ . In the presence of a constant magnetic field, these dynamics conserve the quantities  $\sum_d \mu_d^2$  and  $\sum_d \tau_d^2$ .

The rules replacing (25) determine at each iteration the particle's spin  $s$  among the  $2S+1$  possible values. The general rule reads

$$s[n] = -1 + \frac{1}{S} \sum_{k=1}^{2S} \Theta(s_0 - \tilde{s}_k[n]), \quad \tilde{s}_k := -1 + 2 \sum_{\sigma=-1}^{-1+\frac{k-1}{S}} P(\sigma) \quad (40)$$

where  $\Theta$  is the unit step function and  $P(\sigma) = \mathbb{P}(s = \sigma)$  is the spin pmf. Clearly, (25) is retrieved for  $S = 1/2$ , with  $P(\pm 1) = (1 \pm M)/2$ .

The pmf of spin (a  $2S+1$ -valued discrete random variable) is completely defined by its first  $2S$  central moments. The latter are prescribed by the model as functions of the quantities  $M = \sum_d \mu_d \lambda_d$  and  $T := \sum_d \tau_d \lambda_d$ . The first two central moments read

$$\mathbb{E}[s] = M, \quad (41)$$

$$\mathbb{E}[(s-M)^2] := V = \frac{\sum_d \tau_d^2 - T^2}{2}, \quad (42)$$

with  $\mathbb{E}[(s-M)^3] = -\mathbb{E}[(s-M)^2] \cdot \mathbb{E}[s]$  etc. Overall, we can write  $s[n] = f(M[n], V[n], s_0)$ .

The ER rule (16) is still valid. Additionally,

$$\tau_d \stackrel{\text{ER}}{\leftarrow} \lambda_d \sqrt{\frac{S+1}{S} - s^2} \quad (43)$$

holds. Note that, since  $\sum_d \lambda_d^2 = 1$  by definition, both  $\sum_d \mu_d^2$  and  $\sum_d \tau_d^2$  are constant across an ER.

#### 4.2. Probability densities

For a homogeneous and constant magnetic field, (31) is generalized as follows. Due to the polarization dynamics, the quantities  $M$  and  $T$  do not change with time, thus  $M[n] \equiv M_0$ ,  $T[n] \equiv T_0$ . Similarly,  $\sum_d \mu_d^2$  and  $\sum_d \tau_d^2$  are constant. The transition probabilities are thus constant, too. Since  $s_0$  is attributed to a particle once and for all, the spin  $s$  will stay constant while crossing the magnetic

field  $\lambda$ . Its probability distribution is thus uniquely determined by the values  $M_0$  and  $T_0$ .

For a non-uniform magnetic field (SG apparatus), again the probability distribution of spin is determined at the first ER, that is, at the entry of the SG, and is a function of the quantities  $M_0$  and  $T_0$ . With the ER (43),  $M$  jumps to  $s$  and  $T$  jumps to  $\sqrt{\frac{S+1}{S} - s^2}$ . Consequently, the spin propensity  $\mathbb{E}[s]$  is  $s$  and the variance becomes zero. At the next iteration, the spin will remain constant with probability one. The probability of spins at the exit of the SG is thus uniquely determined by the values  $M_0$  and  $T_0$ .

In the case of two SG in cascade, we have  $\mu_1 = s_1 \lambda_1$  and  $\tau_1 = \lambda_1 \sqrt{\frac{S+1}{S} - s_1^2}$  at the exit of the first SG. Therefore, at the entry of the second SG,  $M_1 = s_1 Y$  and  $V_1 = \left(\frac{S+1}{S} - s_1^2\right) \frac{1-Y^2}{2}$ , having defined  $Y := \sum_d \lambda_{1d} \lambda_{2d} = \cos(\lambda_1, \lambda_2)$ . Accordingly, the spin takes a value  $s_2 = f(M_1, V_1, s_0)$ . After the first ER, the spin propensity jumps to  $s_2$  and the variance jumps to zero. Therefore, at the next iterations, the spin will remain equal to  $s_2$ . Overall, the probability of having a certain spin  $s_2$  at the exit of the second SG depends on  $Y$  and  $s_1$ .

As an example, for  $S = 1$ , the spin pmf is evaluated from the first two moments as

$$P(1) = \frac{V + M^2 + M}{2}, \quad P(0) = 1 - V - M^2, \quad P(-1) = \frac{V + M^2 - M}{2} \quad (44)$$

Thus the spin pdf at the exit of the second SG is

$$\rho(s_2) = (1 - s_2^2) + \frac{s_2}{2} M_1 + \left(-1 + \frac{3}{2} s_2^2\right) (V_1 + M_1^2). \quad (45)$$

Using the expressions for  $M_1$  and  $V_1$  derived above, one obtains

$$\rho(s_2|s_1) = \left(\frac{s_2^2 - s_1^2}{2} - \frac{3}{4} s_1^2 s_2^2\right) + \frac{s_1 s_2}{2} Y + \left(1 - \frac{3}{2}(s_1^2 + s_2^2) + \frac{9}{4} s_1^2 s_2^2\right) Y^2 \quad (46)$$

which precisely match the QM results computed, e.g., in [18]<sup>4</sup>. Further, it can be verified that  $\rho(s_2|s_1) = \rho(s_1|s_2)$ , as it should be.

## 5. Spin Entanglement

In [1] momentum entanglement has been described within the context of the Local-Realistic Model. Here we extend those results to the case of spin entanglement.

---

<sup>4</sup>Cascaded Stern-Gerlach probabilities for higher spin have been seldom studied in the literature. Equations (41)–(42) and, consequently, equations of the type (46), are not present in [18] but have been built upon the general result of that paper.

### 5.1. Particle emission

Entangled particles are emitted at sources as pairs ( $n_R = 2$ ) and denoted with a superscript  $R \in \{I, II\}$ . In addition to assigning entangled momenta ( $v_0^{(I)} + v_0^{(II)} = 0$ ), the source preparation attributes anti-correlated entangled source polarizations and spins, according to the rules

$$\mu_0^{(I)} + \mu_0^{(II)} = 0, \quad s_0^{(I)} + s_0^{(II)} = 0.$$

We shall denote, without loss of generality,  $\mu_0^{(I)} := \mu_0$  and  $s_0^{(I)} := s_0$ . Consequently,  $\mu_0^{(II)} = -\mu_0$  and  $s_0^{(II)} = -s_0$ , where  $\sum_d \mu_{0d}^2 = 1$  and  $s_0 = U[-1, 1]$  as for  $n_R = 1$ .

### 5.2. Microscopic motion

All rules described above remain the same in the case of entangled particles, except for the fact that the quantity  $\tilde{M}^{(R)} := \text{sign}(M^{(R)})|M^{(R)}|^{n_R}$  replaces  $M^{(R)} := \sum_d \mu_d^{(R)} \lambda_d^{(R)}$  in the spin dynamics (25), the magnetic force expression (26) and the magnetic energy (29), which are thus generalized as

$$s^{(R)}[n] = \text{sign}\left(s_0^{(R)} + \tilde{M}^{(R)}[n]\right), \quad (47)$$

$$f_\nu^{(R)}[n] = -\mu_M B_F \tilde{M}^{(R)}[n], \quad (48)$$

$$\mathcal{E}^{(R)}[n] = -\mu_M B_M \tilde{M}^{(R)}[n]. \quad (49)$$

Particularly relevant for what follows is the description of external resets, based on (16) that is still valid. By virtue of its definition above, when  $M^{(R)}$  jumps to  $s^{(R)}$ ,  $\tilde{M}^{(R)}$  jumps to  $\text{sign}(s^{(R)})|s^{(R)}|^2 = s^{(R)}$ . From energy conservation, the reset of momentum in the direction of propagation, equation (50), is now regulated by the coefficient

$$\mathbf{v}_d^{(R)} \stackrel{\text{ER}}{\leftarrow} \alpha^{(R)} \mathbf{v}_d^{(R)} + (1 - \alpha^{(R)}) \nu_d^{(R)} \sum_{d=1}^3 \mathbf{v}_d^{(R)} \nu_d^{(R)}, \quad (50)$$

$$\alpha^{(R)} = \frac{\sum_d (\mathbf{v}_d^{(R)})^2 - \mu_M B_M (s^{(R)} - \tilde{M}^{(R)})}{\sum_d (\mathbf{v}_d^{(R)})^2}. \quad (51)$$

For  $n_R = 1$ , equations of Sect. 3 are clearly retrieved.

### 5.3. Probability densities

We shall evaluate the joint pmf  $\rho(s^{(I)}, s^{(II)})$ , representing the probability that two entangled particles arrive at either of two “detectors” opportunely placed downstream of their respective SG apparatuses in order to intercept the beams with  $s^{(R)} = \pm 1$ .

We note that, experimentally, this pmf and any other related statistics are obtained by counting the coincidences in arrivals at detectors. For this purpose, a data analysis procedure is required to group particles in pairs according to

their arrival times, often using a time-coincidence window. A very thorough and enlightening discussion on this point can be found in [15, 19, 14].

Assuming, without loss of generality, that the settings of the two stations are identical, the arrival times are solely determined by the momentum acquired by the two ensembles of particles in the respective directions of propagation. While source momenta are identical, particles in the two SG's undergo a different momentum reset in the direction of propagation, described by rules (50)–(51). At the entering of the respective SG the spin propensity is  $M^{(R)} = M_0^{(R)} := \sum_d \mu_{0d}^{(R)} \lambda_d^{(R)}$ . While the other parameters of influence are common to both particles, it is therefore the cosine term  $M_0^{(R)} = \cos(\mu_0^{(R)}, \lambda^{(R)})$  that controls the momentum through (51) and ultimately defines the time of arrival at the respective detectors.

For this reason, a coincidence in arrival times is *expectedly* recorded when the two particles have the same value of  $M_0$ , that is, when

$$M_0^{(I)} = \sum_{d=1}^3 \lambda_d^{(I)} \mu_{0d}^{(R)} = \sum_d \lambda_d^{(II)} \mu_{0d}^{(R)} = M_0^{(II)} := M_0 \quad (52)$$

It is now easy to show that, for each selection of  $\lambda^{(I)}, \lambda^{(II)}$ , two values of  $M_0$  fulfill (52), namely,

$$\hat{M}_0 = \pm \sqrt{\frac{1 - \sum_{d=1}^3 \lambda_d^{(I)} \lambda_d^{(II)}}{2}}, \quad (53)$$

having opposite signs and equal probability. Geometrically, these values correspond to the two unit  $\mu_0$  vectors bisecting the angle between the two directions  $\lambda^{(I)}, \lambda^{(II)}$  and co-planar to the same, that is

$$\angle \hat{\mu}_0 = (\angle \lambda^{(I)} + \angle \lambda^{(II)})/2.$$

All other values of  $\mu_0$  give rise to coincidences only with a very small probability and thus do not contribute to the joint pmf.

Similarly to the non-entangled case, inside the SG  $s^{(R)}$  remains constant at the entry value  $\text{sign}(s_0^{(R)} + \text{sign}(M_0)M_0^2)$ . The distributions of  $s^{(R)}$  are therefore found as

$$s^{(I)} = \begin{cases} 1, & s_0 > -\text{sign}(M_0)M_0^2 \\ -1, & s_0 < -\text{sign}(M_0)M_0^2 \end{cases} \quad (54)$$

and

$$s^{(II)} = \begin{cases} 1, & s_0 < \text{sign}(M_0)M_0^2 \\ -1, & s_0 > \text{sign}(M_0)M_0^2 \end{cases} \quad (55)$$

With the help of Fig. 3, we further note that  $\{s^{(I)}, s^{(II)}\} = \{1, 1\}$  for  $s_0 \in [-M_0^2, M_0^2]$  if  $M_0 > 0$ . Likewise,  $\{s^{(I)}, s^{(II)}\} = \{-1, -1\}$  for  $s_0 \in [-M_0^2, M_0^2]$  if  $M_0 < 0$ . Regardless of the sign of  $M_0$ ,  $\{s^{(I)}, s^{(II)}\} = \{-1, 1\}$  for  $s_0 < -M_0^2$  and  $\{s^{(I)}, s^{(II)}\} = \{1, -1\}$  for  $s_0 > M_0^2$ .

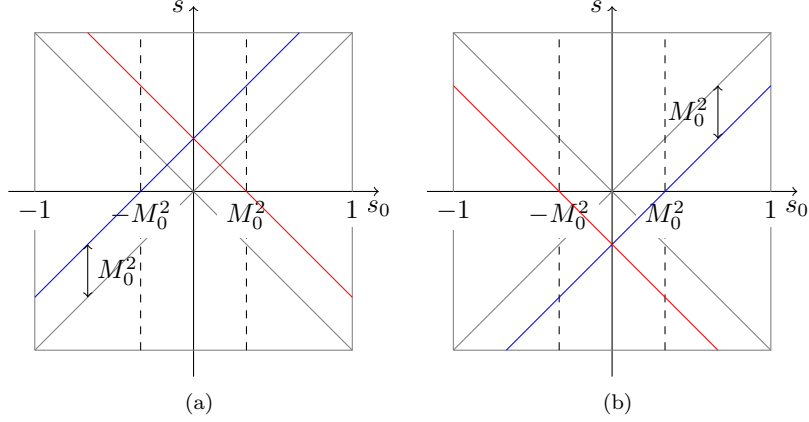


Figure 3: Illustration of the quantities  $s_0^{(I)} + \text{sign}(M_0)M_0^2$  whose sign is  $s^{(I)}$  (blue) and  $s_0^{(II)} + \text{sign}(M_0)M_0^2$  whose sign is  $s^{(II)}$  (red), as a function of  $s_0$ , for  $M_0 > 0$  (a) and  $M_0 < 0$  (b).

Finally, recalling that  $\rho(s_0) = 1/2$ , the joint distribution is evaluated as

$$\rho(1, 1) = \mathbb{P}(M_0 > 0) \cdot \frac{2M_0^2}{2} = \frac{M_0^2}{2} \quad (56)$$

$$\rho(-1, -1) = \mathbb{P}(M_0 < 0) \cdot \frac{2M_0^2}{2} = \frac{M_0^2}{2} \quad (57)$$

$$\rho(1, -1) = \frac{1 - M_0^2}{2} = \rho(-1, 1). \quad (58)$$

Since from (53) the only meaningful value is  $\hat{M}_0^2 = (1 - \cos(\lambda^{(I)}, \lambda^{(II)}))/2$ , the joint distribution reads

$$\rho(s^{(I)}, s^{(II)}) = \frac{1 - s^{(I)}s^{(II)} \cos(\lambda^{(I)}, \lambda^{(II)})}{4}, \quad (59)$$

and the expected value of the product  $s^{(I)}s^{(II)}$  is  $-\cos(\lambda^{(I)}, \lambda^{(II)})$ , that is, precisely the QM prediction.

#### 5.4. Numerical Results

We aim at representing here a textbook two-channel Bell test experiment. A source produces pairs of entangled particles, sent in opposite directions. Each particle beam encounters a SG. Emerging particles from each channel are detected and coincidences in arrivals counted. Similarly to the non-entangled scenario simulated in Sect. 3.3, we shall take  $\lambda^{(R)} = \nu^{(R)}$ , i.e., an inhomogeneity directed along the field in both SG. While the orientation  $\lambda^{(II)}$  is fixed,  $\lambda^{(I)}$  is varied between  $-\pi$  and  $\pi$  in the plane  $x_1-x_3$ . The direction of the two emitted beams is taken as  $\pm x_2$ . Coincidences are registered when particles arrive at



either of a pair of detectors at a distance  $\ell$  from the source at the same time. We assume that the detector sizes in the planes  $x_1$ – $x_3$  are sufficiently large to capture the whole beams leaving the SG regardless of the particles’ deflection.

In the proposed model, particles are emitted at the respective sources according to a Gaussian-wave preparation, with  $m_1 = m_3 = 0$  (see Sect. 3.3), while  $m_2$  would determine the average particle speed along the propagation direction. The initial polarizations are randomly chosen at each emission between  $N_\mu$  possible values, equally spaced between  $\angle\hat{\mu}_0$  and  $\angle\hat{\mu}_0 + 2\pi$ .

Similarly to the single SG scenario, we assume both particle and lattice “training” completed and we simulate the expected-motion version (19)–(20) of the model<sup>5</sup>. In particular, we represent the momentum reset occurring at the ER, (50), by attributing an expected momentum at SG entering that equals  $m_2$ . Consequently, the expected time to arrival is evaluated as

$$\mathbf{T}^{(R)} = \frac{m_2 T_0}{\sqrt{m_2^2 - \mu_B B_M (s^{(R)} - \tilde{M}_0^{(R)})}}. \quad (60)$$

where  $T_0 = \ell/m_2$  is the expected arrival time in the absence of SG. As anticipated in Sect. 5.3, the momentum jump and the consequent time delay depend only on  $M_0^{(R)}$ .

Assuming  $\mu_B M_B \ll m_2^2$ , the expected time delays among arrivals at the two stations are evaluated as

$$\Delta T := \mathbf{T}^{(I)} - \mathbf{T}^{(II)} \approx T_0 \frac{\mu_B B_M}{2m_2^2} (s^{(I)} - s^{(II)}).$$

Accordingly, time arrivals at station I are corrected by adding the value  $\Delta T$  before checking the coincidences.

Ensemble results are compared with QM prediction (59). Figure 4 shows the frequency of the four types of coincidences as a function of the angular difference between the two fields, with  $\mu_M B_F = 0.04$ ,  $N_p = 1 \cdot 10^4$ ,  $N_\mu = 16$ ,  $\ell = 210$ . When compared with the QM predictions, these results confirm the substantial equivalence of the two models as anticipated in the previous section.

### 5.5. Discussion

The previous sections have shown that the proposed model exactly reproduces the joint pmf of a spin-entangled quantum system where coincidences in spin are counted only if they are accompanied by coincidence in arrival time, that is, the regime that Bell test experiments aim to reach [15]. Nevertheless, nowhere in the proposed model, particles, say, II “know” about which magnetic field experience particles I, thus locality applies, certainly together with realism.

---

<sup>5</sup>Contrarily to Sect. 3.3, we renounce using the expected-motion equation (18) and use the full model instead, in order to capture the dispersion of particle arrivals around the average beam centers.

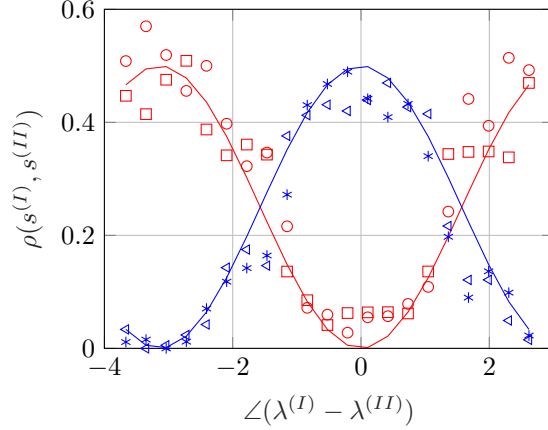


Figure 4: Frequency of coincidences of arrivals (1, 1) (circles), (-1, -1) (squares), (1, -1) (stars), and (-1, 1) (triangles), with their theoretical values  $\rho(1, 1) = \rho(-1, -1)$  (red solid) and  $\rho(1, -1) = \rho(-1, 1)$  (blue solid) as a function of the angle (rad) between  $\lambda^{(I)}$  and  $\lambda^{(II)}$  (Bell experiment, Gaussian-wave beams,  $\mu_M B_F = 0.04$ ,  $N_p = 1 \cdot 10^4$ ,  $N_\mu = 16$ ,  $\ell = 210$ ).

At this point, the reader may wonder why, although  $\mu_0$  and  $s_0$  play the role of “hidden variables” as those explicitly discarded by Bell’s theorem, Bell’s inequalities are violated and the QM statistics are correctly reproduced.

The apparent answer is that the process leading to the pdf (59) does not fall under the form postulated by this theorem<sup>6</sup>. We must consider the fact that, for most choices of  $s_0$  and  $\mu_0$ , no arrival coincidence can be detected. For example, the expected value of the product  $s^{(I)} s^{(II)}$  must be evaluated as

$$\mathbb{E}(s^{(I)} s^{(II)}) = \int_H s^{(I)}(\lambda^{(I)}, s_0, \mu_0) \cdot s^{(II)}(\lambda^{(II)}, s_0, \mu_0) \cdot p_{coi}(\mu_0, \lambda^{(I)}, \lambda^{(II)}) \cdot \rho(s_0) \rho(\mu_0) ds_0 d\mu_0, \quad (61)$$

where  $p_{coi}$  is the probability of coincidence counting, which depends on the respective arrival times of the two particles.

Indeed, (53) states that  $p_{coi} \approx \delta(\mu_0 - \hat{\mu}_0(\lambda^{(I)}, \lambda^{(II)}))$ . The emergence of a particular polarization  $\hat{\mu}_0$  that is a function of both  $\lambda^{(I)}$  and  $\lambda^{(II)}$  results from the fact that for other values of  $\mu_0$ , the desired coincidence of  $T^{(I)}$  and  $T^{(II)}$  at the two stations is impossible or, at least, highly improbable. Thus the counting of coincidences introduces a weighting factor  $p_{coi}$  that ultimately gives rise to the spin-entanglement correlations.

<sup>6</sup>We use Bell’s theorem for deterministic variables here. In fact, the stochastic nature of the model resides in the attribution of the hidden variables, while the relations  $s^{(R)} = f(\mu_0^{(R)}, s_0^{(R)}, \lambda^{(R)})$  as given by (54)–(55) are fully deterministic.

When compared with the Bell definition of hidden variable theory,

$$C_h = \int_H s^{(I)}(\lambda^{(I)}, h) \cdot s^{(II)}(\lambda^{(II)}, h) \cdot \rho(h|\lambda^{(I)}, \lambda^{(II)}) dh ,$$

where  $h := \{s_0, \mu_0\}$  is our set of the *independent* hidden variables<sup>7</sup>, we see that  $\rho(h|\lambda^{(I)}, \lambda^{(II)}) = p_{coi}(\mu_0, \lambda^{(I)}, \lambda^{(II)})\rho(s_0)\rho(\mu_0)$ .

It becomes thus apparent that the Bell assumption  $\rho(h|\lambda^{(I)}, \lambda^{(II)}) = \rho(h)$ , often referred to as “Measurement Independence”, is not satisfied by the proposed model. Therefore, the proposed model is not forbidden by Bell’s theorem, which is based on Bell’s assumptions, to violate Bell’s inequalities.

However, the non-validity of this assumption cannot be explained with the usually solutions (i.e., either non-localism or non-realism), nor with an equally-unpleasant form of (super-)determinism [10]. This motivation to renounce to measurement independence should not either be confused with a detector inefficiency loophole. In the proposed model, the detection process itself is 100% efficient, although the coincidence counting makes that only a fraction of the total entangled pairs of particles concur in building the quantum statistics.

Note that a similar situation was discussed in [1] for momentum-entangled systems, although in that case the two observables (detector positions  $x^{(I)}$  and  $x^{(II)}$ ) are not binary functions. Still, a crucial role is played by the definition of coincidences, in this case based on the simultaneous (expected) arrival of the two particles at localized detectors.

## 6. Conclusions

The paper has shown how nonrelativistic QM including spin can be reproduced by realistic, stochastic, and localistic rules applied to individual particles. QM predictions are indeed retrieved as probability distributions of position, momentum, angular momentum, spin, etc. without appealing to the QM mathematical machinery itself.

To represent spin scenarios, such as Stern-Gerlach apparatuses or a Bell test experiment, the proposed model does not appeal to two-dimensional complex spinors and matrices but uses a relatively simple set of rules, implying that (1) spin is a dichotomic quantity carried on by particles whose value depends on a random source setting and a spin propensity; (2) the latter can vary at each iteration as a function of polarization, which is a three-dimensional attribute, and the magnetic field experienced; (3) polarization is randomly attributed during preparation and has its own rules of variation; it further concurs in determining how particles react to magnetic fields.

Several refinements of the model are still possible. For example, relativistic Newtons second law shall inspire a mechanism to prevent that the momen-

---

<sup>7</sup>We use  $h$  instead of the more common  $\lambda$  to avoid confusion with the magnetic field components.

tum propensity becomes larger than unity under the action of persistent forces. Multi-state and many-particle systems are yet to be fully studied, too.

## References

- [1] Sciarretta A.: A local-realistic model of quantum mechanics based on a discrete spacetime. *Found. Phys.* 48(1), 60–91, (2018).
- [2] Sciarretta, A.: A local-realistic model of quantum mechanics based on a discrete spacetime (extended version) (2017). <https://doi.org/10.13140/RG.2.2.17755.05925>, arXiv:1712.03227.
- [3] Buonomano, V.: Low-Intensity Interference Effects and Hidden-Variable Theories, *Il Nuovo Cimento* 45 B (1), 77–89 (1978).
- [4] Afriat, A., Selleri, F.: The Einstein, Podolski, and Rosen Paradox, in *Atomic, Nuclear, and Particle Physics*, Plenum press, new York (1999).
- [5] Khrennikov, A.: Buonomano against Bell: Nonergodicity or nonlocality?, *Int. Journal of Quantum Information* 15(8):1740010 (2017).
- [6] Nielsen, H.B. and Rohrlich, D.: A path integral to quantize spin. *Nuclear Physics B* 299, 471–483 (1988)
- [7] Dankel, T.: Mechanics on Manifolds and the Incorporation of Spin into Nelson’s Stochastic Mechanics. *Arch. Rational Mech. Anal.* 37, 192–221 (1970)
- [8] Garbaczewski, P.: Randomness in the Quantum Description of Neutral Spin 1/2 Particles, *Fortschr. Phys.* 38(6), 447–475 (1990)
- [9] Buonomano, V.: The EPR paradox and the non-ergodic interpretation of quantum mechanics, in *Quantum Mechanics Versus Local Realism: The Einstein, Podolsky, and Rosen Paradox*, F. Selleri, ed., Plenum, New York, 1988, pp. 327-343.
- [10] Vervoort, L.: Bells Theorem: Two Neglected Solutions, *Found Phys* 43:769791 (2013).
- [11] Mückenheim, W.: A Resolution of the Einstein-Podolsky-Rosen Paradox, *Lett. Nuovo Cimento*, 35(9):300-304, 1982.
- [12] Di Lorenzo, A.: Beyond Bells theorem: admissible hidden-variable models for the spin-singlet. *J. Phys.* 442, 012046 (2013).
- [13] Thompson, C.: The chaotic ball: An intuitive analogy for EPR experiments, *Found. Phys. Lett.*, 9(4):357-382, 1996.
- [14] Michielsen, K., De Raedt, H.: Event-based simulation of quantum physics experiments. *Int. J. Mod. Phys. C* 25(8), 1430003 (2014).

- [15] De Raedt, K., de Raedt, H., Michielsen, K.: A computer program to simulate Einstein-Podolsky-Rosen-Bohm experiments with photons. *Comput. Phys. Commun.* 176(1112), 642-651 (2007).
- [16] Hsu, B., Berrondo, M., Van Huele, J.-F.: Stern-Gerlach dynamics with quantum propagators. *Phys. Rev. A* 83, 012109 (2011).
- [17] Reddy, A., Samuel, J., Shivam, K., Sinha, S.: Coarse Quantum Measurement: An analysis of the SternGerlach experiment, *Phys. Lett. A* 380, 1135-1140 (2016)
- [18] Tekin, B.: Stern-Gerlach Experiment with Higher Spins, *Eur. J. Phys.* 37:035401 (2016).
- [19] Larsson, J.-A., Gill, R. D.: Bells inequality and the coincidence-time loophole, *Europhys. Lett.*, 67(5):707713 (2004).